RSC Advances

PAPER

View Article Online
View Journal | View Issue

Cite this: *RSC Adv.*, 2024, **14**, 689

From waste to energy storage: post-consumer waste expanded polystyrene/rGO composite as a high performance self-standing electrode for coin cell supercapacitors†

S. Vijaya and L. John Kennedy *

This research work aims to explore the potential usage of post-consumer waste expanded polystyrene (EPS) for the fabrication of self-standing electrodes by incorporating reduced graphene oxide (rGO) into it *via* a facile cost-effective mechanical mixing process. The π–π interaction between the expanded polystyrene and rGO is evidenced from FT-IR and Raman analysis. The elevated thermal stability of the EPS/rGO composite from thermogravimetric analysis (TGA) further confirms the interconnection between the rGO and EPS. This π–π stacking interaction between the rGO and the polystyrene molecules present in the polymer matrix enable the composite material to be interconnected throughout which is beneficial for the charge transport process. The symmetric coin cell supercapacitor fabricated using the EPS/rGO composite electrode can be operated with a high operating voltage of 1.6 V in aqueous KOH and Na_2SO_4 electrolytes. The devices fabricated with KOH and Na_2SO_4 electrolytes deliver an areal capacitance of 11.9 mF cm^{-2} and 10 mF cm^{-2} at the discharge current density of 0.1 mA cm^{-2}. Further, the devices fabricated with the KOH and Na_2SO_4 electrolytes demonstrated remarkable rate capability of 87.1% and 99.5% after 10 000 continuous charge discharge cycles. This facile method of preparation without consuming energy or polluting the environment is a novel approach which can be scaled-up to large-scale fabrication of self-standing plastic electrodes for low-cost energy storage applications.

Received 17th October 2023
Accepted 9th December 2023

DOI: 10.1039/d3ra07071a

rsc.li/rsc-advances

1. Introduction

Technology advancement in consumer electronics highly demands portable energy storage devices. Carbon materials are widely studied for energy storage applications since they are abundant, low-cost materials, having high specific capacitance and high power density and being electrochemically stable materials.[1] In recent years, storing energy in plastics is a new concept in the field of energy storage in which low-cost plastic materials are employed for energy storage applications.[2] Often research communities have attempted to convert the plastic and industrial waste materials into carbon materials which can be used as electrode materials for supercapacitors.[3] In our day-to-day life, polymers, particularly expanded polystyrene (EPS) which is commonly known as thermocol, a synthetic aromatic polymer material, are most commonly used in the form of packaging materials, foam cups, shock absorbing materials, transportation, medicine *etc.*[4,5] The usage of EPS is increasing continuously and subsequently the disposal of the same in the environment is also increasing rapidly. After use, it is thrown into open spaces which is harmful to the environment. Disposal or burning processes of EPS are not advisable as they can release toxic chemicals which can pollute the land and ecosystem. Instead, converting them into value added products such as adhesive materials for construction, or for preparing carbon materials, has been a welcomed effort to reduce the pollution.[6] Nevertheless, an eco-friendly recycling process is required for a better environment.[7] Waste EPS can be dissolved in organic solvents such as petrol, acetone, ethanol or combinations of them to make useful products like adhesive or glue which can be used in construction, factories *etc.*[4] In the field of energy storage, Vadiyar *et al.* converted the EPS waste into carbon materials for the preparation of a carbon-Fe_3O_4 nanocomposite for application in a supercapacitor.[8] Though, using them directly without consuming energy or polluting the environment for the energy application is a novel approach. Basically, polystyrene (PS) is an electrical insulator, however, the conductivity of the polystyrene can be tuned by the addition of conducting carbon materials like graphene, rGO *etc.* into it.[9] The incorporation of the carbon materials into the non-conductive plastic materials is an effective way to make the

Materials Division, School of Advanced Sciences, Vellore Institute of Technology, Chennai, Tamil Nadu, India. E-mail: ljkennedy14@gmail.com

† Electronic supplementary information (ESI) available. See DOI: https://doi.org/10.1039/d3ra07071a

conductive polymer composites.[10] Such a process of incorporating the conducting material into the polymer matrix is a ground-breaking technique which is also beneficial to improve the mechanical, thermal, optical and electrical properties of the desired composite.[9,11] The adhesive and charge transfer properties of the polymer were significantly improved *via* π–π interaction of phenyl rings present in the graphene.[12,13] Many attempts including *in situ* polymerization, *in situ* reduction, solution blending, and melt blending were made for the preparation of polymer/graphene composites.[12] For instance, the encapsulation of Ag nanoparticles into the polymer matrix showed improved thermal stability, mechanical strength and anti-bacterial property.[5] Likewise, the polystyrene/graphene composite prepared *via* melt blending showed enhanced electrical properties.[14] Similar to this, polystyrene grafted on rGO *via* an emulsion polymerization method showed improved dielectric behavior of the composite.[15] An analytical device fabricated with a polystyrene@rGO composite prepared *via* an electrostatic interaction process showed promising performance for the application of biosensors.[16] The mechanical mixing of the EPS with the rGO at high rpm can prevent the agglomeration of the rGO over EPS which is advantageous for the continuous interconnected network.[10] A polystyrene/rGO composite prepared by a casting technique showed electrical conducting properties (conductivity in the range of 10^{-11} to 10^{-6} S m^{-1}) thus can be used in electronic devices.[9] The conductivity of the polystyrene/rGO composite was improved to 22.68 S m^{-1} while prepared *via* a two-step *in situ* reduction. These results confirmed that the rGO formed a connected network with the polymer matrix to improve the conductivity and this composite can be a potential candidate for the application of electronic and energy storage devices.[17] Kwon *et al.*[18] showed the presence of non-covalent π–π stacking between the basal plane of the graphene and backbone of the aramid (aromatic polyamide) nanofiber. They form hydrogen bonding with the oxygen functional groups present in the graphene molecule and the amide groups (CO═NH) present in the aramid polymer which improved the mechanical strength as well as the electrochemical stability of the composite. The highest specific capacitance of the symmetric coin cell fabricated with an graphene/aramid composite electrode using 6 M KOH achieved was 207 F g^{-1} at the current density of 0.5 A g^{-1}. After introducing the abundant functional groups into the carbon fiber paper, the symmetric cell constructed with those functionalized self-standing carbon fiber paper electrodes delivered an areal capacitance of 370 mF cm^{-2} at the current density of 50 mA cm^{-2} in 1 M Na_2SO_4 electrolyte.[18] Conducting polymer polypyrrole (PPy) composites with rGO have been extensively studied for supercapacitor applications due to their synergistic effect which resulted in longer cycle life, higher specific capacitance and higher energy density compared to pure PPy.[19]

Based on the literature, in this research work, we aim to convert the post-consumer EPS waste into a self-standing electrode by incorporating rGO into it for supercapacitor applications. This is an extremely simple, yet a new approach to employ the non-conducting waste polymer material which is harmful to the environment for energy storage applications. The electrochemical performance of the composite was studied in most frequently used acidic, alkaline and neutral electrolytes. The as fabricated electrode displays unique capacitive behavior and extremely long-life cycle. The symmetric coin cell supercapacitor devices based on EPS/rGO electrodes constructed with 6 M KOH electrolyte was evaluated for maximum areal energy and power density. Further, for practical application demonstration, two coin cells were connected in series that can glow an red LED over 5 minutes. This new way of constructing the EPS based self-standing electrode is an efficient yet cost effective approach to produce a potential candidate for the low-cost energy storage devices. This study is an approach towards "waste to worth" concept.

2. Experimental

2.1 Materials

Waste expanded polystyrene (EPS), otherwise known as thermocol, was collected from a dump yard at VIT Chennai campus. Acetone, KOH, Na_2SO_4, and H_2SO_4 were purchased from Merck and used as purchased without further modifications. Commercial rGO was purchased from Adnano Technology. LIR 2032 coin cell case with spacer and spring were purchased from Xiamen Aot Electronics Technology Co., Ltd., China.

2.2 Preparation of EPS/rGO composite

Firstly, large pieces of EPS were shredded into small pieces with the help of mixer. Those collected small spheres were weighed and used directly without any further modifications. Different compositions of EPS and rGO were prepared. The weight ratios of EPS : rGO were 2 : 1, 1 : 1 and 1 : 2 respectively. All the compositions of EPS and rGO were prepared by following the same process. Briefly, the calculated amount of rGO (as per the desired weight ratio) was mixed with acetone in a mechanical mixer. Afterwards, calculated amount of shredded EPS (as per the desired weight ratio) was added and mixed evenly with the rGO. The resulted black colored, soft jelly like EPS/rGO composite was collected and spread into a sheet/film with the help of a glass rod. Finally, the composite was dried at ambient room temperature to evaporate the solvent and thus obtained self-standing EPS/rGO electrode. They were further cut into small pieces for other characterizations. The pristine EPS sheet/film was also prepared by following the same procedure without adding rGO for comparison purpose. It is noted that the weight ratio of EPS : rGO 1 : 2 does not form self-standing electrode. It was found that at this particular ratio, intactness between EPS and rGO was affected due to the poor gel formation and eventually led to discontinuous network between EPS and rGO despite regular mixing procedures of these individual compounds. Instead, the fabricated electrode samples withered to powder form, hindering the formation of self-standing electrode with desired size and shape. However, the compositions of EPS : rGO with 2 : 1 and 1 : 1 were formed jelly like composite which can be used for the formation of self-standing electrode with desired size and shape.

2.3 Characterization

The Fourier Transform Infrared Spectroscopic (FT-IR) analysis of the pure rGO and EPS/rGO composite was performed using FT-IR JASCO, Japan. The Raman spectrum was recorded by employing invia Raman microscopes from Renishaw (wavelength of the laser used is 532 nm). The thermogravimetric analysis (TGA) of the samples was obtained by Inkarp thermogravimetric analyzer at the heating rate of 10 °C min^{-1} under nitrogen atmosphere. The contact angle measurement of pure EPS and EPS/rGO composite was analyzed against water by KYOWA interFAce Measurement and Analysis System FAMAS by Sessile drop method. The surface morphology of the samples was performed by Thermo Fisher Field Emission Scanning Electron microscope (FE-SEM). The surface chemical composition of the pristine EPS and EPS/rGO films were conducted by Physical Electronics XPS Systems.

2.4 Electrochemical characterization

The as prepared EPS/rGO composite was directly used as electrodes. The electrochemical investigations such as cyclic voltammetry (CV), galvanostatic charge discharge (GCD) studies of the electrodes were performed using PARSTAT 4000 (Princeton) electrochemical analyzer. The CV of the electrode was performed in a conventional three electrode system in which EPS/rGO electrode served as a working electrode, Ag/AgCl as a reference electrode, and a Pt wire as a counter electrode. The CV, GCD, and EIS studies were conducted in 1 M KOH, 1 M H_2SO_4 and 1 M Na_2SO_4 solutions respectively. The electrochemical impedance spectroscopic studies were conducted in the frequency range of 0.1 to 10^5 Hz with the amplitude of the sinusoidal AC voltage of 10 mV. The equivalent circuit diagram was fitted using ZSimpWin software. Symmetric coin cells were fabricated in which EPS/rGO composite served as both anode and cathode, while Whatman filter paper served as a separator. The components of the coin cells were a cell case covering for top and bottom, spring ring, metal plate, two identical EPS/rGO composite electrodes. The diameter of the EPS/rGO electrode was 16 mm and the area of the device calculated was 4.022 cm^2 (for both electrodes). Whatman filter paper soaked in electrolytes (6 M KOH, 1 M H_2SO_4 and 1 M Na_2SO_4) overnight was used as separator while fabricating the coin cell.

3. Results and discussions

Different compositions of EPS and rGO were prepared in the ratio of 2 : 1, 1 : 1, 1 : 2. Pristine EPS/rGO was also prepared for comparison purpose. The EPS/rGO in the ratio 1 : 2 does not form self-standing electrode due to the poor gel formation. Therefore, the weight ratio of EPS : rGO in 2 : 1 and 1 : 1 were considered for further studies. Photographs of the prepared pristine EPS film and EPS/rGO with various compositions are shown in Fig. S1.† For initial studies, coin cell supercapacitor devices were constructed using EPS/rGO composite self-standing electrodes (prepared with the weight ratio of EPS : rGO in 2 : 1 and 1 : 1) in which 6 M KOH was served as electrolyte. From the CV and GCD studies shown in Fig. S2a and b,† it is observed that the device fabricated with 2 : 1 ratio of EPS : rGO delivered low performance (an areal capacitance of 1.6 mF cm^{-2} at the current density of 0.05 mA cm^{-2}) due to the low amount of rGO in the EPS matrix. Therefore, further studies were conducted and discussed throughout this paper for the EPS/rGO

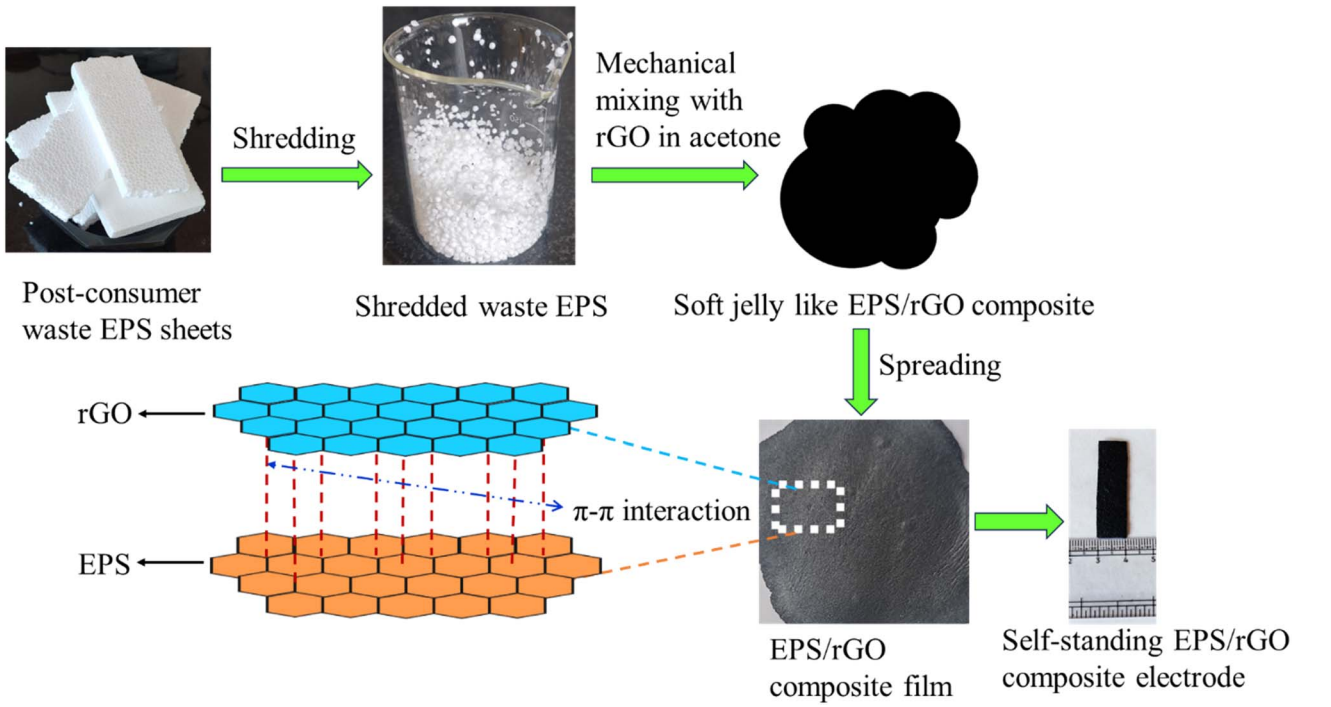

Fig. 1 Schematic representation of EPS/rGO electrode fabrication.

composite sample prepared with 1 : 1 ratio. The schematic representation of the preparation of EPS/rGO composite is shown in the following Fig. 1.

The existence of functional groups in EPS/rGO composite and their interfacial interaction was investigated using FT-IR technique. The FT-IR spectrum (Fig. 2a) of rGO shows the symmetric stretching of –O–H bonding at 3426 cm^{-1}. The absorption bands at the wavenumber of (1725, 1575, 1091) cm^{-1} are corresponding to the vibrations of C–H and C–O groups present in the rGO. Further, the band at 794 cm^{-1} represents the out of plane bending vibration of C–H group belong to the benzene ring.[20] The sharp absorption band at 694 cm^{-1} indicates the π–π interaction between the both graphene oxide and polystyrene molecule present in the composite. Along with this absorption band, the characteristic absorption peaks corresponding to C–H vibrations of the benzene ring present in the EPS/rGO composite are also observed at (747, 903, 1025, 1450, 1491, 1599) cm^{-1}.[20] Further, from the literature, it is observed that the presence of peak at 1025 cm^{-1} is owing to the π–π stacking interaction of the both graphene oxide and polystyrene.[21] The presence of both symmetric and asymmetric vibrations of the methylene group present in the EPS can be identified by the presence of peaks at (2918, 2851) cm^{-1}.[22] The stretching vibrations of C–H bands at (3061, 3024) cm^{-1} are associated with the polystyrene.[23] It is worthy to note that these peaks are not observed in the FT-IR spectrum of the rGO. Thus, the presence of interfacial interaction between both the EPS and rGO is evidenced from the FT-IR results. Further, the results are consistent with the literature and it strongly supports the formation of EPS/rGO composite which is having interconnected network.

Raman technique was employed to analyze the structural, chemical compositions, non-covalent π–π stacking of the rGO and polystyrene molecules present in the EPS/rGO composite. From the Raman spectrum shown in Fig. 2b, two characteristic D and G bands of pure rGO can be seen at 1350 cm^{-1} and 1580 cm^{-1} which are ascribed to sp^3 and sp^2 hybridized carbon atoms. The intensity ratio of the D and G band indicates the quantity of sp^3 hybridized carbon atoms over sp^2 hybridized carbon atoms. Here, the intensity ratio I_D/I_G of the EPS/rGO composite is increased to 0.539 compared to the pure rGO (0.418) owing to the surface π–π interaction of the benzene rings of EPS and basal plane present in the rGO.[16] Overall, the increase in the D and G band ratio indicates the increase of sp^3 hybridized carbon atoms over sp^2 hybridized carbon atoms in the EPS/rGO composite. The peaks present at 620, 793, 1000, 1030, 1154 cm^{-1} are ascribed to the polystyrene molecule present in EPS/rGO composite.[20,24] These results are consistent with the FT-IR analysis of the EPS/rGO composite.

The thermal stability of the EPS and EPS/rGO composite samples were examined by TGA analysis. From the thermograms shown in Fig. 2c, the thermal stability of rGO is observed until 600 °C without noticeable degradation. The EPS sample starts decomposition at 412 °C whereas the EPS/rGO starts at 434.9 °C. The EPS/rGO composite showing elevated thermal stability compared to pure EPS sample because of the presence of interconnected rGO in the sample. After 400 °C, both EPS and EPS/rGO samples undergo thermal degradation and beyond 450 °C, EPS decomposed completely into its monomers, dimers and trimers.[9]

The surface morphology of the pure rGO and EPS/rGO samples were analyzed by FE-SEM technique. Fig. 2d and e shows the well-arranged nanosheet morphology of the pure rGO. Similar nanosheet morphology of the EPS/rGO composite can be seen in Fig. 2f and g. The interconnected network of the EPS/rGO composite is obtained by the simple mechanical

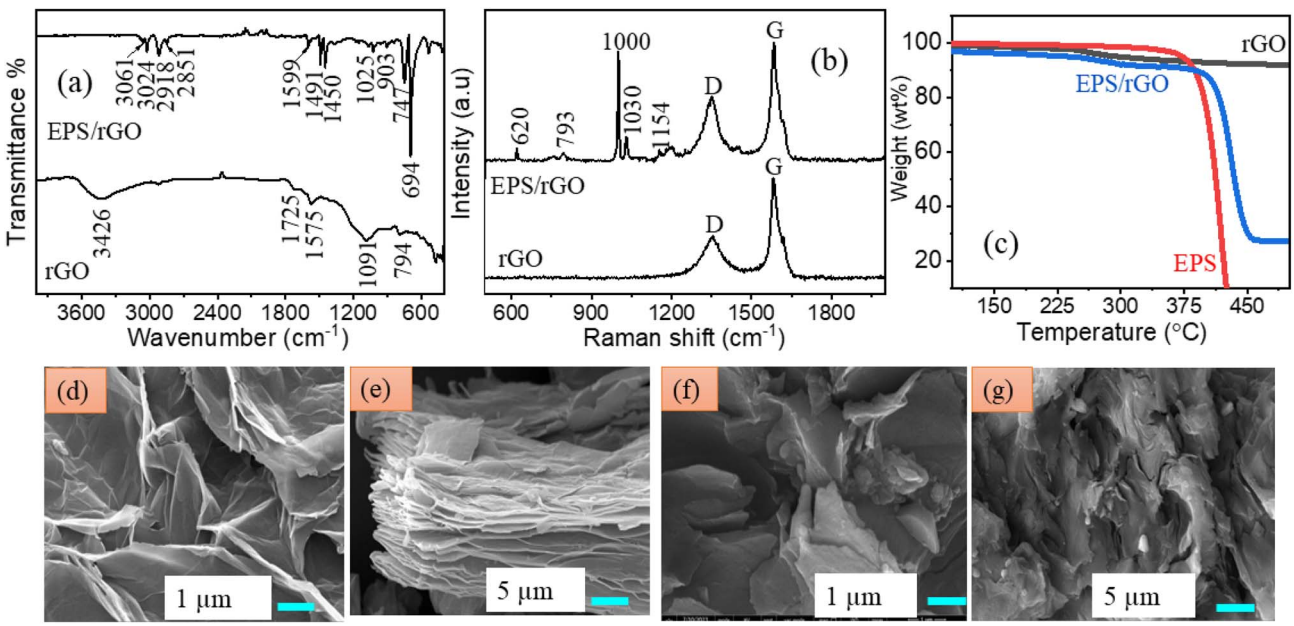

Fig. 2 (a) FT-IR (b) Raman spectrum of pure rGO and EPS/rGO composite (c) TGA curves of rGO, EPS, EPS/rGO (d, e) FE-SEM images pure rGO (f, g) FE-SEM images of EPS/rGO composite.

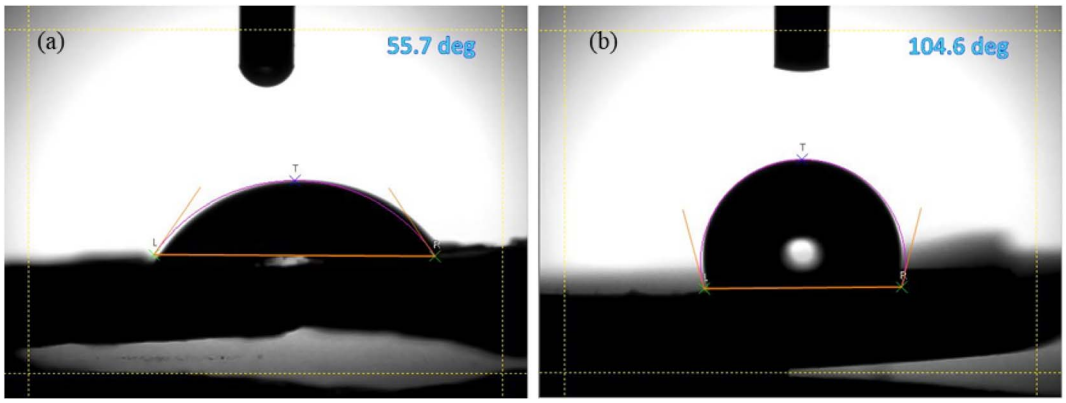

Fig. 3 The contact angles of (a) pristine EPS (b) EPS/rGO composite.

blending process. The sheet like morphology of the EPS/rGO composite clearly demonstrates the rGO incorporation into the EPS matrix. Since the FE-SEM image of the pure form of EPS shown in Fig. S3† displays approximately plane surface morphology, the sheet like morphology is mainly contributed by the rGO present in the sample. Moreover, Fig. 2f and g confirms the continuous network of the composite which ensures the uniform distribution of the rGO into the EPS sheet. This has the major impact on the device performance.

The wettability of the surface of the pure EPS and EPS/rGO composite was performed by measuring the static contact angle of water droplet on their surface. The water droplet on pristine EPS and EPS/rGO composite are shown in Fig. 3a and b. The high static angle of 104.6° which is much higher than the

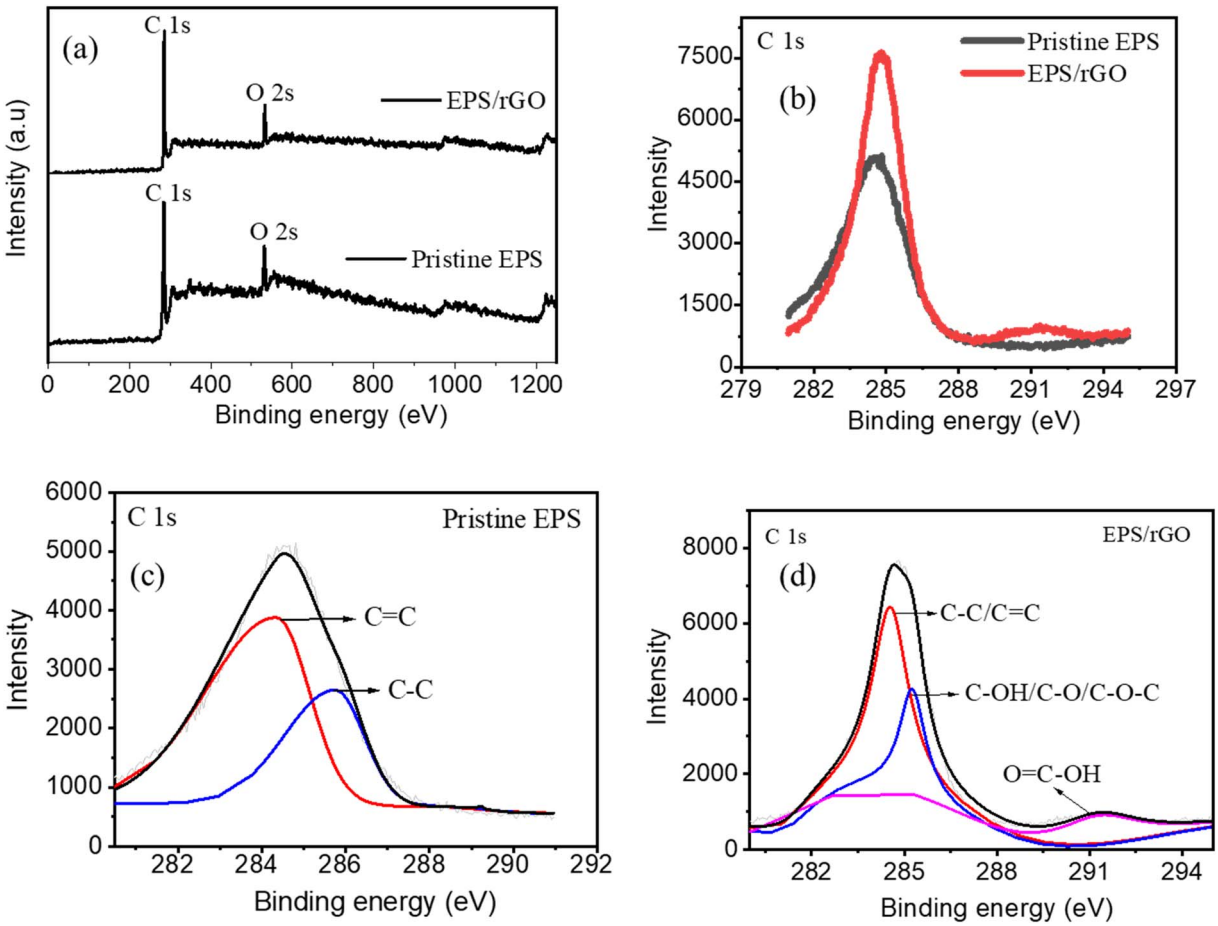

Fig. 4 (a) XPS spectra of pristine EPS and EPS/rGO composite (b) comparison of C 1s spectrum of pristine EPS and EPS/rGO composite (c) C 1s spectrum of pristine EPS (d) C 1s spectrum of EPS/rGO composite.

pure EPS (55.7°) demonstrates the increasing hydrophobicity of the EPS/rGO composite film. This dramatic increase in hydrophobicity validates the abundant availability of the rGO on the composite surface[25] which is hydrophobic in nature due to the absence of polar functional groups. Further, the increase in hydrophobicity is advantageous to prevent the accumulation of moisture into the polymer matrix surface which ensures the long-term stability of the composite films under ambient conditions.[26]

The surface composition and chemical states of the pristine EPS and EPS/rGO films were investigated by XPS analysis. The corresponding XPS spectra of both the samples are shown in Fig. 4a–d. Though no oxygen group is present in the pristine EPS film, the peak corresponding to O 1s is observed in the survey spectrum of same (Fig. 4a). The reason is the possibility of presence of surface absorbed oxygen from air[27] since the air molecule can easily be trapped into the holes present in the EPS film. The comparison of the C 1s spectrum of both pristine EPS film and EPS/rGO (Fig. 4b) confirms the successful incorporation of the rGO into the EPS matrix. Further, the peak intensity of the EPS/rGO composite is higher than the pristine EPS which suggest that the increased C–C, C=C bonds in the composite (originated from EPS). The deconvoluted C 1s spectrum of pristine EPS film (Fig. 4c) shows two peaks at 284.5 eV and 285.4 eV respectively. Those peaks are corresponding to C=C of the phenyl ring and C–C of the EPS polymer.[28] Similarly, the presence of peaks at 284.5, 286.3, 291 eV in the deconvoluted C 1s spectrum of EPS/rGO composite film (Fig. 4d) confirms the existence of C–C/C–H/C=C, C–OH/C–O/C–O–C, O=C–OH within the composite which further supports the successful incorporation of the rGO into the EPS matrix.[29]

A systematic electrochemical investigation of the EPS/rGO electrode was conducted in a three-electrode system in which a Pt wire served as a counter electrode and Ag/AgCl as a reference electrode using three different electrolytes such as 1 M KOH, 1 M H_2SO_4 and 1 M Na_2SO_4. The as prepared EPS/rGO

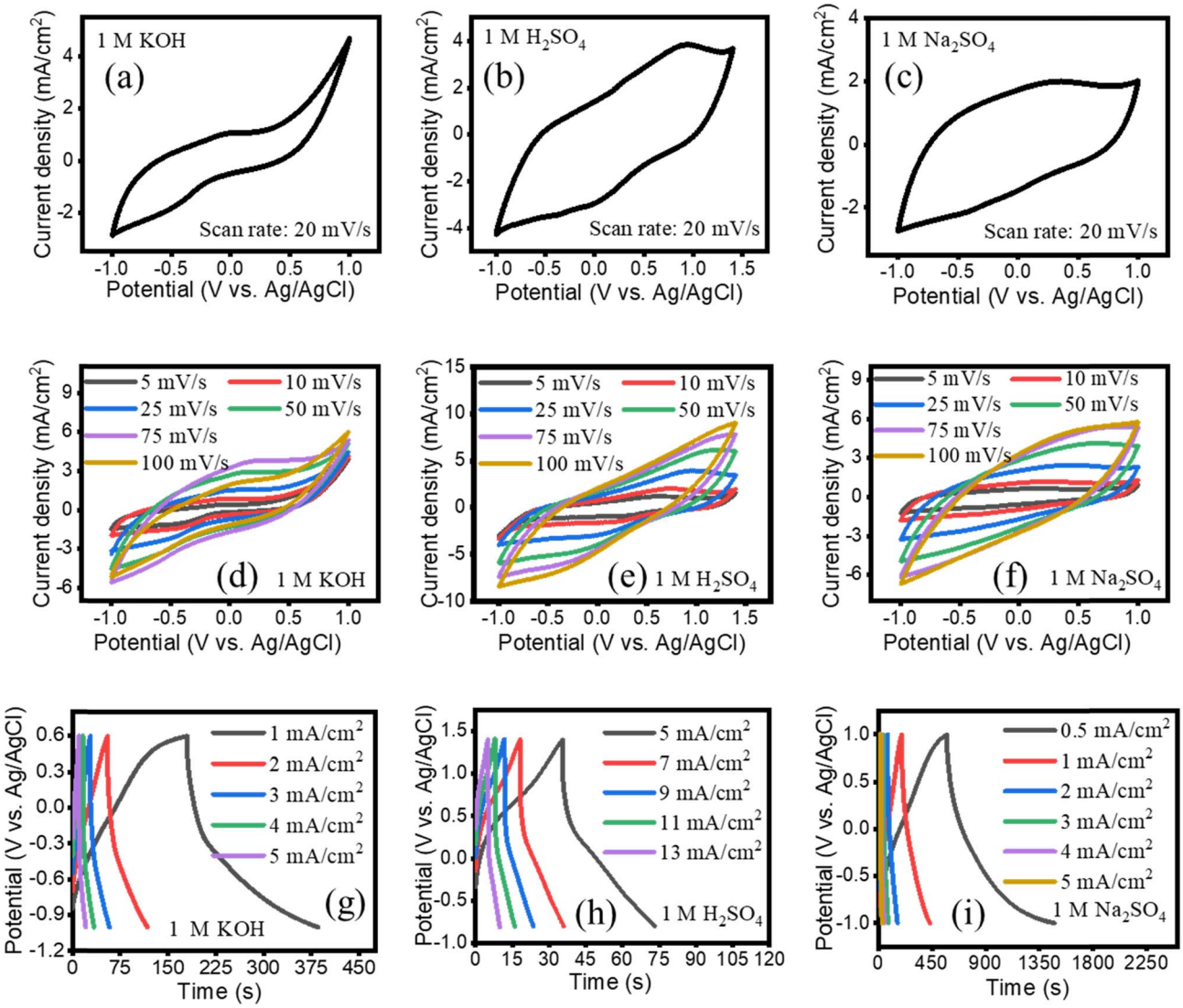

Fig. 5 (a, b, c) CVs at 20 mV s^{-1} (d–f) CVs at various scan rates (g–i) GCD of EPS/rGO composite recorded in 1 M KOH, 1 M H_2SO_4, Na_2SO_4 aqueous electrolyte.

composite was cut into pieces as per required sizes and directly used as a working electrode. The area under the curve is increased for both H_2SO_4 and Na_2SO_4 compared to KOH electrolyte which is evidenced from the CV plot (Fig. 5a–c) recorded at the scan rate of 20 mV s^{-1}. This indicates the increase in capacitive behavior of the electrode in H_2SO_4 and Na_2SO_4 electrolyte. Moreover, the shape of the CV plot recorded in aqueous H_2SO_4 and Na_2SO_4 suggests that the electrode is a suitable candidate to act as both anode and cathode.

The absence of the redox peaks in the CV curve suggests that the capacitance of the electrode is mainly due to the contribution of electrical double layer capacitance.[30] However, in this work, the EPS/rGO electrode shows more pronounced redox reaction in H_2SO_4 solution indicating the enhanced faradaic charge transfer reaction which might come from the presence of functional groups in rGO.[31] This result suggests the existence of pseudocapacitive behavior along with electrical double layer capacitance behavior of the electrode. Thus, the resulted areal capacitance value of the EPS/rGO electrode with 1 M H_2SO_4 exhibited superior charge storage capacity (117 mF cm^{-2}) compared to 1 M KOH (74 mF cm^{-2}) and 1 M Na_2SO_4 (95 mF cm^{-2}) electrolytes. The increase in current density while increasing the scan rates implicates the good rate capability of the electrode in all three electrolytes (Fig. 5d–f). The interactions of the H^+ ion with the functional group present in the rGO is given as follows[31]

$$\text{–COOH} \leftrightarrow \text{–COO} + H^+ + e^-$$

$$\text{>C–OH} \leftrightarrow \text{>C=O} + H^+ + e^-$$

$$\text{>C=O} + e^- \leftrightarrow \text{>C–O}^-$$

The electrochemical capacitive behavior of the EPS/rGO composite electrodes are investigated by GCD measurements.

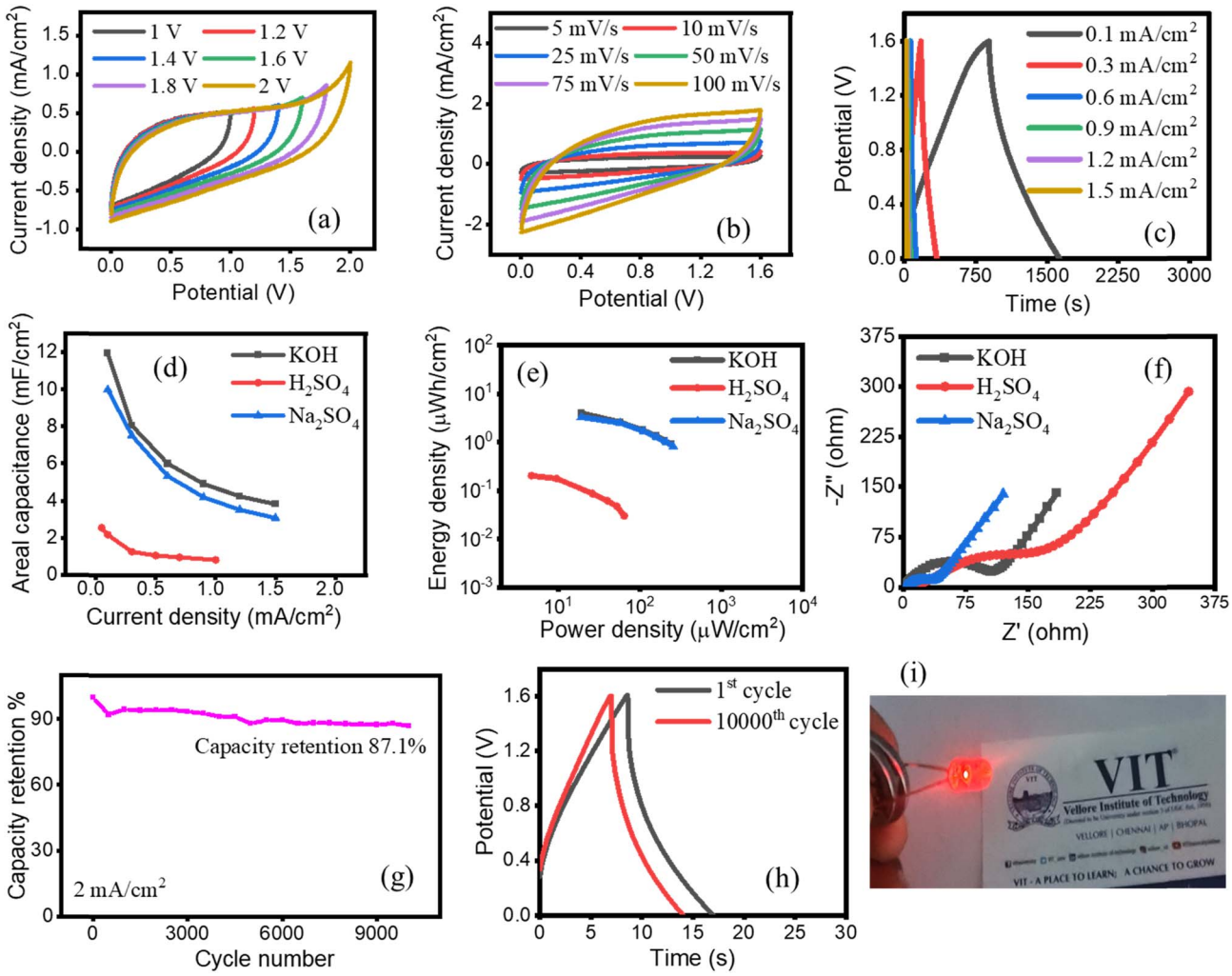

Fig. 6 Studies of EPS/rGO symmetric coin cell fabricated in 6 M KOH: (a) CVs at varied voltage window (b) CVs at varied scan rates (c) GCDs at varied current densities. Studies of EPS/rGO symmetric coin cell fabricated in 6 M KOH, 1 M H_2SO_4, 1 M Na_2SO_4 (d) areal capacitance with respect to the discharge current (e) Ragone plots (f) Nyquist plots. Studies of EPS/rGO symmetric coin cell fabricated in 6 M KOH: (g) capacity retention of the EPS/rGO symmetric coin cell in 6 M KOH (h) comparison of 1st and 10 000th GCD profile (i) photograph of LED powered by serially connected two EPS/rGO symmetric coin cells with 6 M KOH.

The GCDs of the EPS/rGO electrode recorded at different current densities are shown in Fig. 5g–i. The shape of the GCD profiles measured in all three electrolytes (KOH, H_2SO_4, Na_2SO_4) is not a perfect triangle, which features the existence of pseudocapacitive nature of the electrode. This result is consistent with the CV profiles of the EPS/rGO electrodes in all three electrolytes (KOH, H_2SO_4, Na_2SO_4). From the GCD plot, the EPS/rGO electrode in aqueous Na_2SO_4 solution delivers 476 mF cm^{-2} at the discharge current density of 0.5 mA cm^{-2}, which is highest among aqueous solution of KOH (143 mF cm^{-2} at 1 mA cm^{-2}) and H_2SO_4 (152 mF cm^{-2} at the current density of 5 mA cm^{-2}). The *iR* drop increases with increasing the current densities as reported in the previous literature.[32] From the GCD profiles, it is found that the *iR* drop is more pronounced with the H_2SO_4 solution compared to the other KOH and Na_2SO_4 electrolytes at the discharge current density of 5 mA cm^{-2}. The *iR* drop relates the resistance experienced by the electrode in the electrolyte and loss of energy during charging/discharging process.[33] From the Nyquist plots of EPS/rGO electrodes shown in Fig. S4,† it is observed that the diameter of the semicircle (R_{ct}) for the EPS/rGO electrode in H_2SO_4 electrolyte is highest compared to the other electrolytes KOH and Na_2SO_4 due to the blocked diffusion path of ions.[34] Because of this high R_{ct}, the EPS/rGO electrode in H_2SO_4 electrolyte shows high *iR* drop compared to KOH and Na_2SO_4 electrolytes. Further, the high *iR* drop of the EPS/rGO electrode in H_2SO_4 contributes to the quick discharge capacity of the electrode and can be observed from the GCD plot shown in Fig. 5h. In the fixed voltage window, the *iR* drop contributes to the lower usable voltage as evidenced from the GCD plot of the coin cell supercapacitor device fabricated with EPS/rGO in H_2SO_4 electrolyte.

Further, for practical applications, symmetric coin cell LIR 2032 supercapacitors based on EPS/rGO electrodes were fabricated with two identical electrodes. A Whatman filter paper was used as a separator. All three aqueous KOH, H_2SO_4, and Na_2SO_4 electrolytes were used for the fabrication of coin cell supercapacitor devices. The electrochemical behavior of all the devices were examined by CV, GCD and EIS techniques. The operating voltage range of the devices were investigated by performing CV analysis at potential range from 0 to 2 V at a scan rate of 20 mV s^{-1}. Fig. 6a shows the well capacitive behavior of the EPS/rGO electrode in aqueous KOH (Na_2SO_4 is shown in Fig. S4a†). Further, the CV profile shows the quasi-rectangular shape. The linear increase in the capacitance with the wide potential window (0 to 2 V) demonstrates the good electrochemical stability[35] of the EPS/rGO electrode in KOH and Na_2SO_4 electrolytes as well. However, this trend is not followed in the case of H_2SO_4 electrolyte (Fig. S5a†). The charge storage capacitance of the device is investigated by CV technique at various scan rates from 5 to 100 mV s^{-1} (Fig. 6b). The increase in current density while increasing the scan rate indicates the predominant rate capability of the device. The same trend is observed for the coin cell fabricated with H_2SO_4 electrolyte (Fig. S5b†) and Na_2SO_4 electrolyte (Fig. S4b†). Moreover, the quasi-rectangular shape is retained for all three electrolytes even at a high scan rate demonstrates the excellent capacitive behavior of the electrode. The charge transport within the electrode and at electrode/electrolyte interfaces are further investigated by GCD technique. The GCD profiles (Fig. 6c) for the KOH electrolyte exhibits mixed plateau-like and triangular like shapes due to the contribution of both faradaic and non-faradaic charge storage mechanisms. The similar mixed plateau-like and triangular like shapes of the GCD plot are observed in Na_2SO_4 and H_2SO_4 electrolytes (Fig. S4c and S5c†). The EPS/rGO coin cell supercapacitor fabricated in aqueous KOH electrolyte demonstrated superior charge storage capacitance (areal capacitance of 11.9 mF cm^{-2}) followed by Na_2SO_4 electrolyte (areal capacitance of 10 mF cm^{-2}) at the discharging current density of 0.1 mA cm^{-2} compared to the H_2SO_4 electrolyte (areal capacitance calculated is 2.5 mF cm^{-2} at the current density of 0.05 mA cm^{-2}). These results demonstrate the good capacitive behavior of the EPS/rGO electrode in both KOH and Na_2SO_4 solutions. However, a better areal capacitance of the KOH based device compared to Na_2SO_4 based one is due to the higher molar conductivity of K^+ ion compared to that of Na^+ ion in the electrolyte[36] yet the overall performance is comparable. The high operational potential window 0 to 1.6 V was achieved for the device fabricated with KOH and Na_2SO_4 electrolytes. The aqueous H_2SO_4 based device shows narrower potential window 0 to 0.8 V similar to the previous literature.[31] It is worthy to be noted here is the presence of different functional groups and their quantity in rGO is the deciding factor of the capacitive behavior of the rGO based electrode.[37] The maximum energy and power density of the EPS/rGO coin cell supercapacitor can reach 3.9 μW h cm^{-2} and 243 μW cm^{-2} which is noticeably better than the coin cells fabricated with H_2SO_4 (0.2 μW h cm^{-2} and 63.9 μW cm^{-2}) and Na_2SO_4 (3.2 μW h cm^{-2} and 256.9 μW cm^{-2}) electrolytes respectively. The decrease in areal capacitance with the increase in current density of the EPS/rGO electrode is observed from Fig. 6d for the devices fabricated with all three aqueous KOH, H_2SO_4 and Na_2SO_4 electrolytes. At low current density, the distribution of the ions present in the electrolyte is uniform and thus the ions can easily penetrate into the active sites of the electrode surface. While at the high current density, the difficulty in the penetration of the ions resulted in the decrease in capacitance of the device.[38] Further, at high current density, there is energy loss due to heat during the charge/discharge process[38] which have negative impact on the areal capacitance of the device. However, moderate decrease in areal capacitance with the increase in current density of the EPS/rGO electrode in H_2SO_4 compared to KOH and Na_2SO_4 electrolytes is observed due to the rapid transfer of the ions present in the electrolyte solution.[39] The energy and power density are important parameters to determine the energy storage capacity of the supercapacitors. Ragone plots are used to evaluate those parameters. The Ragone plot of the EPS/rGO electrode fabricated with all three aqueous KOH, H_2SO_4 and Na_2SO_4 electrolytes shown in Fig. 6e illustrates the superior performance of the supercapacitor device fabricated with aqueous KOH and Na_2SO_4 electrolytes compared to those with H_2SO_4 electrolyte. In Nyquist plot, the intercept on the real axis represents the series resistance (R_S) contributed by electrolyte, electrode, cell components. CPE1 (constant phase element), CPE2 represent the nonideal capacitance in the double layer at

electrode/electrolyte interfaces due to the surface roughness, imperfections in the electrode surface. R_{CT1} is located at the high frequency region of the semicircle corresponding to the electrolyte ion diffusion at the electrode/electrolyte interface and conductivity of the electrode whereas R_{CT2} corresponds to the charge transfer resistance at the low frequency region of the semicircle. The Z_W represents Warburg impedance which relates the diffusion of the electroactive species into the electrode surface.[33] Though the H_2SO_4 electrolyte in a three-electrode system exhibits lowest solution resistance (shown in Fig. S6†) due to its highest ionic conductivity compared to K^+ and Na^+ ions, the coin cell fabricated with it shows highest solution resistance.[36] Fig. 6f shows the coin cell constructed with KOH and Na_2SO_4 solution show lower R_s value of 6.94 Ω and 8.53 Ω compared to H_2SO_4 which shows 43.08 Ω indicating the lower electrolyte resistance experienced by the device fabricated with KOH and Na_2SO_4 electrolytes. Further, both the devices fabricated with the electrolytes KOH and Na_2SO_4 display similar kind of Warburg like behavior. The equivalent circuit of the EIS parameter analysis is shown in Fig. S7.† The electrochemical stability of the electrode is the deciding factor for the real-time application of the device. Fig. 6g shows the long-term electrochemical stability of the device fabricated with KOH electrolyte through 10 000 continuous cycles of GCD at a current density of 2 mA cm^{-2}. Initially, the device shows the decrease in capacitance till it reaches around 500 cycles then the capacitance started increase and maintained until 10 000 cycles. The device shows the best cycling performance with 87.1% capacity retention. The long-term electrochemical stability of the other devices fabricated with Na_2SO_4 and H_2SO_4 electrolytes show better capacity retention of 99.5% and 94.5% (Fig. S4d and S5d†). Overall, the device fabricated with the Na_2SO_4 electrolyte shows the best capacitance retention of 99.5% after 10 000 cycles. These results are further evidenced from the CV plots (Fig. S8a–c†) measured initial and after 10 000 cycles. The CV curve shows negligible degradation of the EPS/rGO electrode in all three KOH, H_2SO_4 and Na_2SO_4 electrolytes indicating the good rate capability of the devices. To clarify this, the GCD plot of the 1st and 10 000th cycles are compared in Fig. 6h. Finally, for real time applications, two EPS/rGO symmetric coin cells constructed with 6 M KOH electrolyte connected in series and tested with red LED (Fig. 6i).

The observed performances of EPS/rGO electrode constructed in both conventional three electrode and coin cell supercapacitor devices in three electrolytes KOH, H_2SO_4 and Na_2SO_4 are briefly explained as follows. Firstly, the performance of the EPS/rGO electrode is highly depended on the influence of the electrolytes used.[40] Further, it is well known that the capacitance obtained for two electrode system is half the capacitance obtained from a three electrode system[41,42] due to the difference in the electrode capacitance contribution. Thus, it is expected that the capacitance of the two electrode device is lower than the capacitance obtained from a three electrode configuration as reported in literatures.[41,42] In similar way, the capacitance values obtained in our work for the EPS/rGO electrode fabricated as coin cell supercapacitor are 11.9, 10, 2.5 mF cm^{-2} for the electrolytes KOH, Na_2SO_4 and H_2SO_4 respectively. However, the EPS/rGO electrode in a three electrode system are 74, 95, 117 mF cm^{-2} for the electrolytes KOH, Na_2SO_4 and H_2SO_4 respectively. Though EPS/rGO electrode in H_2SO_4 electrolyte delivers highest capacitance value of 117 mF cm^{-2} in a three electrode system due to the interaction of functional groups in rGO with the electrolyte,[31,43] the GCD of the same shows high iR drop which comes from the high internal resistance.[32,33] According to the literature,[44] as the voltage value increases, the contribution of capacitance due to pseudocapacitive component also increases. The EPS/rGO in a three electrode system with H_2SO_4 delivers high capacitance value (117 mF cm^{-2}) along with high potential window of −0.8 to 1.4 V (Fig. 5h). The pseudocapacitive behavior of the EPS/rGO electrode is because of the oxygen containing rGO which is evidenced from the XPS results (Fig. 4). However, in coin cell supercapacitor fabricated with H_2SO_4, the CV plot shows the absence of pseudocapacitive behavior at least till 1 V of potential window (Fig. S5b†). As the symmetric device fabricated with H_2SO_4 electrolyte can reach only upto 0.8 V during charge–discharge process (Fig. S5c†), it is believed that the capacitance value of the device is poor due to the lack of contribution of capacitance by pseudocapacitive components present in rGO yet the device shows better capacity retention (94.4%) than the device constructed with KOH (87.1%).

Further, the areal capacitance for coin cells with different electrolytes were found to be in the order of KOH > Na_2SO_4 > H_2SO_4. In a three electrode system, the GCD of the EPS/rGO electrode shows less *iR* drop for KOH and Na_2SO_4 electrolytes compared to H_2SO_4 electrolyte. Because of the large *iR* drop of the EPS/rGO electrode in H_2SO_4 electrolyte, the usable voltage of the same in coin cell is drastically decreased (the voltage window for the H_2SO_4 device is only 0 to 0.8 V). However, it is observed that the voltage window of the EPS/rGO coin cell device in both KOH and Na_2SO_4 electrolytes is 0 to 1.6 V. In addition to this, the EIS analysis of the EPS/rGO coin cell fabricated with aqueous electrolytes shows that the R_s value of the device in KOH solution is lowest compared to the other Na_2SO_4 and H_2SO_4 electrolytes. The low R_s value leads to the improved capacitance of the devices.[33] The R_s value of the devices follows the order of KOH < Na_2SO_4 < H_2SO_4 which further supports their performances.

From the previous reports, it is observed that the polyelectrolyte-wrapped graphene/carbon nanotube core-sheath fibres,[45] polypyrrole (PPy)/GO nanocomposite,[33] carbon dot@graphite felt-600,[46] rGO FCSC (flexible cable-type supercapacitor)[47] delivered an areal energy density of 3.84, 13.56, 20.7, 5.3 μW h cm^{-2} with the areal power density of 20, 500, 150, 509 μW cm^{-2}. The energy and power density of the coin cell supercapacitor fabricated in our work with EPS/rGO electrode in KOH electrolyte resulted in 3.9 μW h cm^{-2} and 243 μW cm^{-2} respectively. The energy density values achieved are comparable with the spun yarn supercapacitors made from polyelectrolyte-wrapped graphene/carbon nanotube core-sheath fibres (3.84 μW h cm^{-2}). However, the power density achieved by this EPS/rGO is 10 times higher than the spun yarn supercapacitors (20 μW cm^{-2}). The comparison of the areal energy and power

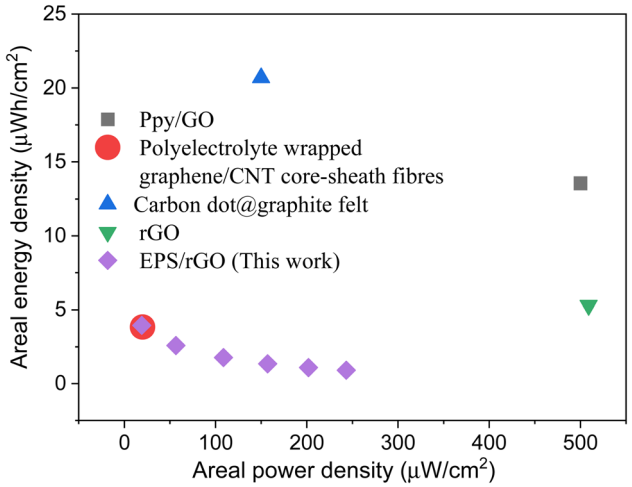

Fig. 7 Ragone plot compared with literature.

density of this work with the reported values and as shown in the Ragone plot in Fig. 7.

For real time applications, two different symmetric coin cell devices, D1 (device 1) and D2 (device 2) were connected in series or parallel. The GCD of the same was performed at a current density of 1 mA cm^{-2}. From the GCD plots displayed in Fig. 8, the obtained areal capacitance value for individual device D1 is 1.78 mF cm^{-2} and for the device D2 is 0.72 mF cm^{-2}. While the calculated areal capacitance for the devices connected in series is 0.58 mF cm^{-2} and for the devices connected in parallel is 3.37 mF cm^{-2} respectively. The increase in capacitance while the devices connected in parallel connection demonstrates the practical way of increasing the overall capacitance of the devices.[48] Moreover, the predicted areal capacitance value for the device connected in series and parallel is 0.51 mF cm^{-2} and 2.5 mF cm^{-2} which is approximately equals the calculated areal capacitance values.

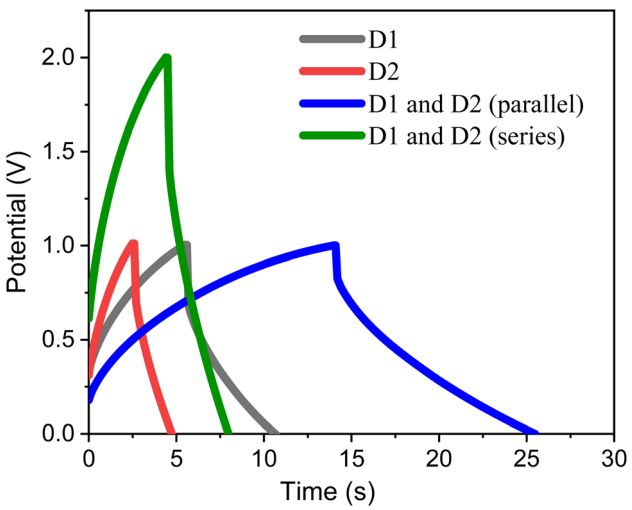

Fig. 8 GCD curves recorded for two different symmetric coin cell supercapacitor devices (D1 and D2) connected in parallel and series at a current density of 1 mA cm^{-2}.

4. Conclusion

Post-consumer EPS waste is successfully converted into a self-standing electrode by incorporating conductive rGO *via* a facile one-step mechanical mixing for the application of supercapacitors. The increased I_D/I_G ratio observed in Raman analysis for the EPS/rGO composite confirmed the existence of the π–π interaction between the phenyl rings of EPS and basal plane present in the rGO. The elevated thermal stability of the EPS/rGO composite compared to a pure EPS sample was due to the uniform distribution of rGO in the EPS matrix through the interconnected network. The as fabricated conducting EPS/rGO composite electrode delivered an areal capacitance in the electrolytes of the order KOH > Na_2SO_4 > H_2SO_4. The order of rate capability was 99.5%, 94.4%, and 87.1% for Na_2SO_4, H_2SO_4, and KOH electrolytes respectively after 10 000 cycles with a high operating voltage of 1.6 V (KOH and Na_2SO_4 only). Two symmetric coin cells fabricated with a self-standing EPS/rGO composite electrode connected in series are capable of lighting up a red LED for more than 5 minutes, demonstrating the promising next generation polymer electrode for supercapacitor applications. This new approach of utilizing EPS waste for energy storage applications can pave a way for large-scale production of self-standing polymer electrodes for multifunctional applications in various energy research sectors.

Author contributions

S. Vijaya: conceptualization, methodology, investigation, validation, data curation, writing – original draft, L. John Kennedy: writing – review & editing.

Conflicts of interest

There are no conflicts to declare.

Acknowledgements

The first author thanks the Vellore Institute of Technology (VIT) Chennai, Tamil Nadu, India for providing a post-doctoral fellowship.

References

1 H. P. Cong, X. C. Ren, P. Wang and S. H. Yu, *Energy Environ. Sci.*, 2013, **6**, 1185–1191.
2 M. E. Abdelhamid, A. P. O'Mullane and G. A. Snook, *RSC Adv.*, 2015, **5**, 11611–11626.
3 W. Utetiwabo, L. Yang, M. K. Tufail, L. Zhou, R. Chen, Y. Lian and W. Yang, *Chin. Chem. Lett.*, 2020, **31**(6), 1474–1489.
4 A. S. Kukde and B. D. Lade, *Int. J. Innov. Res. Technol.*, 2021, **7**, 206–210.
5 S. S. Bag, A. Bora and A. K. Golder, *Polym. Compos.*, 2021, **42**, 6094–6105.
6 A. N. Uttaravalli, S. Dinda and B. R. Gidla, *Process Saf. Environ. Prot.*, 2020, **137**, 140–148.

7 N. B. Selukar, C. V. Lande and C. G. Ingole, *Int. J. Innov. Res. Adv.Eeng.*, 2014, **1**, 98–100.
8 M. M. Vadiyar, X. Liu and Z. Ye, *ChemSusChem*, 2018, **11**, 2410–2420.
9 S. H. Alrefaee, A. B. G. Trabelsi, A. E. Abdelhamid, A. A. Ward, W. Elsharkawy, F. H. Alkallas, A. M. Mostafa, A. N. Al-Ahmadi, S. S. Nafee, R. A. Pashameah and A. M. Khalil, *J. Mater. Res. Technol.*, 2023, **25**, 2631–2640.
10 Z. Tu, J. Wang, C. Yu, H. Xiao, T. Jiang, Y. Yang, D. Shi, Y. W. Mai and R. K. Li, *Compos. Sci. Technol.*, 2016, **134**, 49–56.
11 P. Xavier, K. Sharma, K. Elayaraja, K. S. Vasu, A. K. Sood and S. Bose, *RSC Adv.*, 2014, **4**, 12376–12387.
12 W. Deng, G. Li, W. Li, M. Yang and W. Cui, *Des. Monomers Polym.*, 2023, **26**, 23–30.
13 D. Zhao, G. Zhu, Y. Ding and J. Zheng, *Polymers*, 2018, **10**, 716.
14 B. Shen, W. Zhai, C. Chen, D. Lu, J. Wang and W. Zheng, *ACS Appl. Mater. Interfaces*, 2011, **3**, 3103–3109.
15 T. Zhang, W. Huang, N. Zhang, T. Huang, J. Yang and Y. Wang, *Eur. Polym. J.*, 2017, **94**, 196–207.
16 Q. Lan, H. Shen, J. Li, C. Ren, X. Hu and Z. Yang, *Chem. Commun.*, 2020, **56**, 699–702.
17 N. Wu, X. She, D. Yang, X. Wu, F. Su and Y. Chen, *J. Mater. Chem.*, 2012, **22**, 17254–17261.
18 S. R. Kwon, J. Harris, T. Zhou, D. Loufakis, J. G. Boyd and J. L. Lutkenhaus, *ACS Nano*, 2017, **11**, 6682–6690.
19 O. B. Abdillah, Y. B. Rus, M. Ulfa and F. Iskandar, *J. Energy Storage*, 2023, **74**, 109300.
20 Z. G. Mohammadsalih and N. S. Sadeq, *Fuller. Nanotub. Carbon Nanostructures.*, 2022, **30**, 373–384.
21 G. Yin, Z. Zheng, H. Wang, Q. Du and H. Zhang, *J. Colloid Interface Sci.*, 2013, **394**, 192–198.
22 S. H. Alrefaee, A. B. G. Trabelsi, A. E. Abdelhamid, A. A. Ward, W. Elsharkawy, F. H. Alkallas, A. M. Mostafa, A. N. Al-Ahmadi, S. S. Nafee, R. A. Pashameah and A. M. Khalil, *J. Mater. Res. Technol.*, 2023, **25**, 2631–2640.
23 S. S. Bag, A. Bora and A. K. Golder, *Polym. Compos.*, 2021, **42**, 6094–6105.
24 X. Hu, Z. Xu, K. Li, F. Fang and L. Wang, *Appl. Surf. Sci.*, 2015, **355**, 1168–1174.
25 Y. Li, Y. Zhang, H. Zhang, T. L. Xing and G. Q. Chen, *RSC Adv.*, 2019, **9**, 4180–4189.
26 J. Wu, J. Wang, X. Huang and H. Bai, *Energy Environ. Sci.*, 2018, **11**, 1280–1286.
27 S. Huan, L. Bai, G. Liu, W. Cheng and G. Han, *RSC Adv.*, 2015, **5**(63), 50756–50766.
28 H. Gu, C. Ma, C. Liang, X. Meng, J. Gu and Z. Guo, *J. Mater. Chem. C*, 2017, **5**(17), 4275–4285.
29 N. Wu, X. She, D. Yang, X. Wu, F. Su and Y. Chen, *J. Mater. Chem.*, 2012, **22**(33), 17254–17261.
30 R. K. Mishra, G. J. Choi, Y. Sohn, S. H. Lee and J. S. Gwag, *Chem. Commun.*, 2020, **56**, 2893–2896.
31 Y. Zhu, S. Cheng, W. Zhou, J. Jia, L. Yang, M. Yao, M. Wang, P. Wu, H. Luo and M. Liu, *ACS Appl. Mater. Interfaces*, 2017, **9**, 13173–13180.
32 K. Yousefipour, R. Sarraf-Mamoory and A. Yourdkhani, *Surf. Interfaces*, 2022, **29**, 101638.
33 J. Wen, Y. Ding, J. Zhong, R. Chen, F. Gao, Y. Qiao, C. Fu, J. Wang, L. Shen and H. He, *RSC Adv.*, 2020, **10**, 41503–41510.
34 K. Yousefipour, R. Sarraf-Mamoory and S. Mollayousefi, *RSC Adv.*, 2022, **12**(43), 27868–27876.
35 K. Krishnamoorthy, P. Pazhamalai and S. J. Kim, *Energy Environ. Sci.*, 2018, **11**, 1595–1602.
36 F. Barzegar, D. Y. Momodu, O. O. Fashedemi, A. Bello, J. K. Dangbegnon and N. Manyala, *RSC Adv.*, 2015, **5**, 107482–107487.
37 Y. J. Oh, J. J. Yoo, Y. I. Kim, J. K. Yoon, H. N. Yoon, J. H. Kim and S. B. Park, *Electrochim. Acta*, 2014, **116**, 118–128.
38 K. Yousefipour, R. Sarraf-Mamoory and A. Yourdkhani, *Colloids Surf. A Physicochem. Eng. Asp.*, 2022, **647**, 129066.
39 B. Fang and L. Binder, *J. Phys. Chem. B*, 2006, **110**(15), 7877–7882.
40 C. Zhong, Y. Deng, W. Hu, J. Qiao, L. Zhang and J. Zhang, *Chem. Soc. Rev.*, 2015, **44**, 7484–7539.
41 M. D. Stoller and R. S. Ruoff, *Energy Environ. Sci.*, 2010, **3**, 1294–1301.
42 S. Roldán, D. Barreda, M. Granda, R. Menéndez, R. Santamaría and C. Blanco, *Phys. Chem. Chem. Phys.*, 2015, **17**, 1084–1092.
43 R. Yadav, P. Joshi, M. Hara, T. Yana, S. Hashimoto and M. Yoshimura, *SN Appl. Sci.*, 2020, **2**, 1–13.
44 V. Ruiz, S. Roldán, I. Villar, C. Blanco and R. Santamaría, *Electrochim. Acta*, 2013, **95**, 225–229.
45 L. Kou, T. Huang, B. Zheng, Y. Han, X. Zhao, K. Gopalsamy, H. Sun and C. Gao, *Nat. Commun.*, 2014, **5**, 3754.
46 Y. Chen, D. Huang, L. Lei, S. Chen, X. Liu and M. Cheng, *Nanoscale*, 2021, **13**, 4995–5005.
47 G. K. Veerasubramani, K. Krishnamoorthy, P. Pazhamalai and S. J. Kim, *Carbon*, 2016, **105**, 638–648.
48 H. Ma, B. Guo, W. Wu, Z. Zhang and R. Zhang, *J. Energy Storage*, 2022, **55**, 105696.